Dehydration-activated structural phase transition in a two-dimensional hybrid double perovskite

Rui-Ying Ren,‡[a] Chang-Yuan Su,‡*[ab] Ting Shao,[a] Zhi-Xu Zhang,[b] Pei-Zhi Huang,[a] Yi Zhang,[b] Qiang-Qiang Jia*[a] and Da-Wei Fu*[a]

*(a Institute for Science and Applications of Molecular Ferroelectrics, Key Laboratory of the Ministry of Education for Advanced Catalysis Materials, Zhejiang Normal University, Jinhua, 321004, People's Republic of China.
b Ordered Matter Science Research Center, Jiangsu Key Laboratory for Science and Applications of Molecular Ferroelectrics, Southeast University, Nanjing, 211189, People's Republic of China.)*

Table of contents

Experimental Measurement Methods

DSC Measurements.

DSC measurement of $[C_6H_{14}N]_4CuBiI_8 \cdot H_2O$ was executed from 303 to 473 K at a rate of 5 K min^{-1} applying a PerkinElmer Diamond DSC instrument.

Single-Crystal X-ray Crystallography.

Variable-temperature single-crystal XRD data of $(CHA)_4CuBiI_8 \cdot H_2O$ and $(CHA)_4CuBiI_8$ were collected using a Bruker APEX-II CCD with MoKα radiation (λ = 0.71073 Å) at 150 K, 400 K and 150 K (after cooling) whose processing was disposed by the APEX3. Variable-temperature crystal structures were solved using a direct method and subsequent continuous Fourier synthesis. Subsequently, these crystals were refined by full-matrix leastsquares methods based on F2 using the SHELXLTL software package. Eventually, in addition to the asymmetric units and packing shown in main body using DIAMOND software, other relevant crystallographic data and structure refinement are listed in Table S2 in supporting information.

Since the standard space group (*C*2/*c* No. 15) was not used in the CCDC (1903595) originally reported by Zheng et al., we re-uploaded this structure as follows: CCDC: 2167267 ($(CHA)_4CuBiI_8 \cdot H_2O$ at 150 K). In addition, CCDC of $(CHA)_4CuBiI_8$ at 400 K and 150 K is 2120152 and 2120153, respectively.

Powder X-Ray Diffraction.

Powder X-Ray diffraction (PXRD) data for $(CHA)_4CuBiI_8 \cdot H_2O$ and $(CHA)_4CuBiI_8$ were measured on a D8 Advance03030502 X-ray diffractometer at room temperature. Diffraction patterns were collected in the 2θ range of 5−55° with a step size of 0.02°.

Thermogravimetric analysis.

Thermogravimetric analysis (TGA) was executed to observe the heat stability of $(CHA)_4CuBiI_8 \cdot H_2O$ and $(CHA)_4CuBiI_8$ using a TA Q50 system at a heating rate of 10 K min^{-1} from room temperature to 1000 K in the atmosphere.

Ultraviolet-visible (UV-vis) absorbance spectroscopy.

Ultraviolet–visible (UV–vis) absorbance spectroscopy was measured on polycrystalline samples by using Shimadzu (Tokyo, Japan) UV-2600 spectrophotometer at room temperature.

Dielectric Measurements.

Firstly, the dry crystals $(CHA)_4CuBiI_8$ were grinded into powder, which was pressed into a sheet subsequently. Using the conductive carbon paint and wires, the thin plate was made into capacitor measured for dielectric measurements. The complex dielectric constants ($\varepsilon = \varepsilon' - i\varepsilon''$, where ε' is the real part, and ε'' represents the imaginary parts) were measured by a TongHui TH2828A instrument with a temperature range of 300−400 K.

Hirshfeld surfaces analysis.

Hirshfeld surfaces and the related 2D-fingerprint plots were calculated by using the CrystalExplorer program with inputting structure file in CIF format. In this work, all the Hirshfeld surfaces were generated using a standard (high) surface resolution. The 3D Hirshfeld surfaces and 2D fingerprint plots are unique for any crystal structure. The intensity of molecular interaction is mapped onto the Hirshfeld surface by using the respective red-blue-white scheme: where the white or green regions exactly correspond to the distance of Van der Waals contact, the blue regions correspond to longer contacts, and the red regions represent closer contacts. In 2D fingerprint plots, each point represents an individual pair (d_i, d_e), reflecting the distances to the nearest atom inside (d_i) and outside (d_e) of the Hirshfeld d_{norm} surface.

The normalized contact distance d_{norm} is based on d_e, d_i and the van der Waals (vdW) radii of the two atoms external (r_e^{vdW}) and internal (r_i^{vdW}) to the surface:

$$d_{norm} = \frac{d_i - r^{vdW}}{r_i^{vdW}} + \frac{d_e - r}{r_e^{vdW}}$$

d_{norm} surface is used for the identification of close intermolecular interactions.
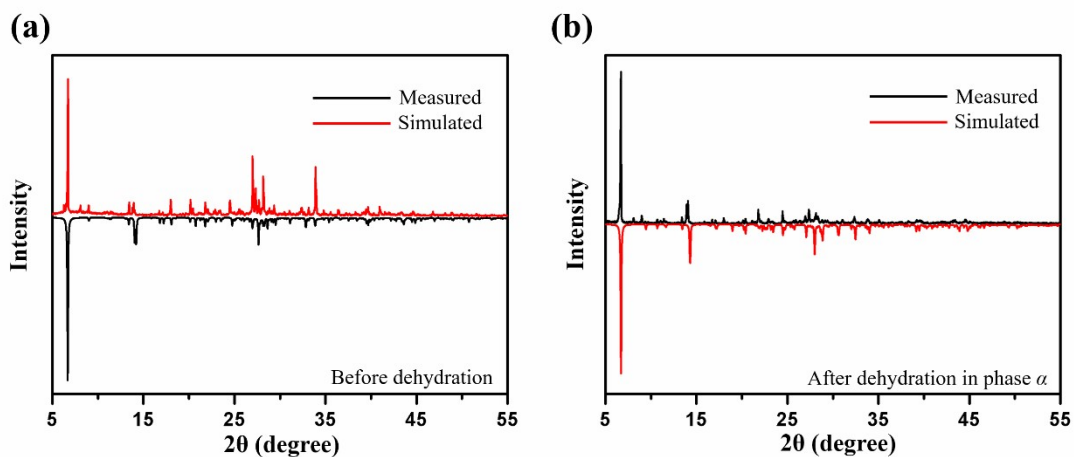
Figure S1. Measured and simulated powder X-ray diffraction patterns of (CHA)$_4$CuBiI$_8$·H$_2$O (a) and (CHA)$_4$CuBiI$_8$ at room temperature (b).
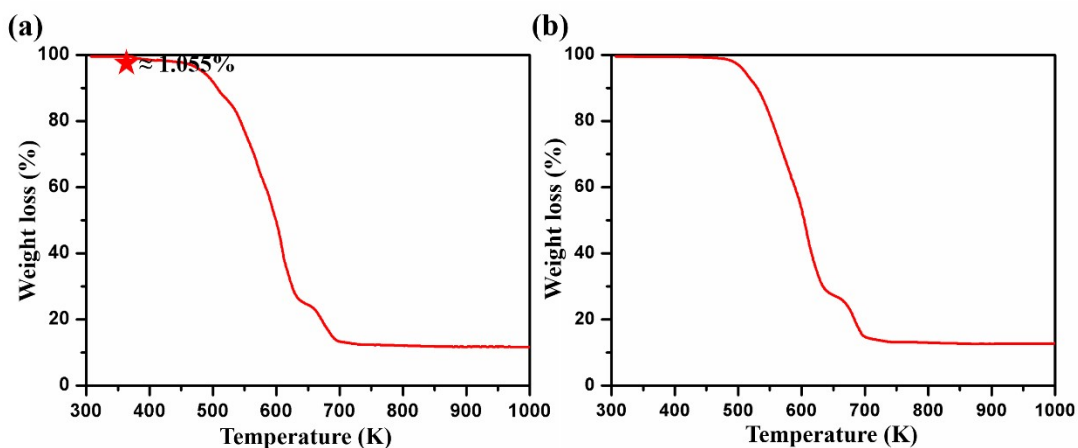
Figure S2. TGA curve of (CHA)$_4$CuBiI$_8$·H$_2$O (a) and (CHA)$_4$CuBiI$_8$ (b).
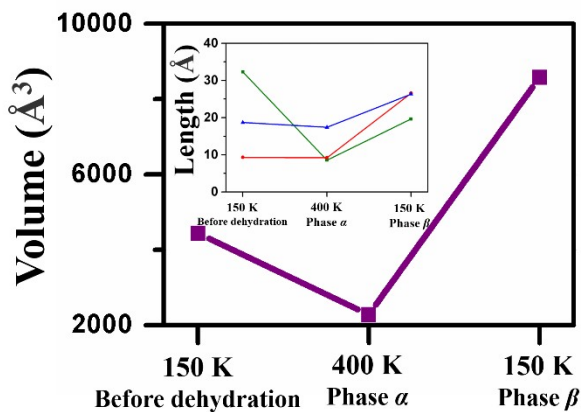
Figure S3. Changes in cell parameters of (CHA)$_4$CuBiI$_8$·H$_2$O at 150 K and (CHA)$_4$CuBiI$_8$ at 400 K and 150 K including Volume and *a*, *b*, *c* (inset).
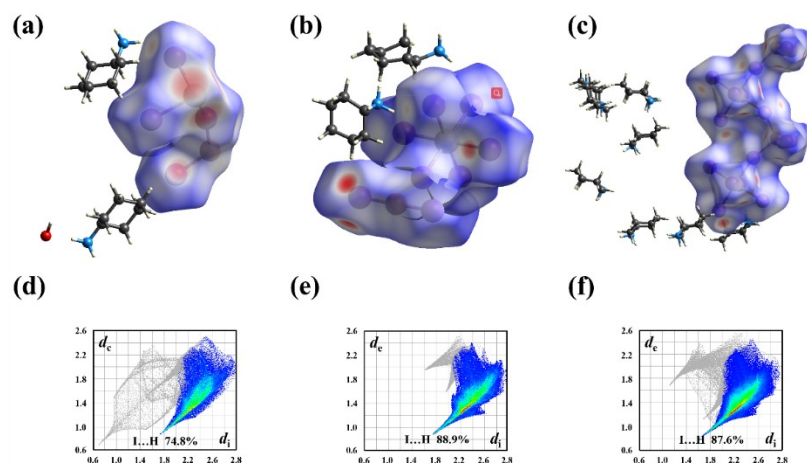
Figure S4. Comparison for Hirshfeld dnorm surfaces and two-dimensional (2D) fingerprint plots of $(CHA)_4CuBiI_8 \cdot H_2O$ at 150 K (a)(d), and $(CHA)_4CuBiI_8$ at 400 K (b)(e) and 150 K (c)(f).
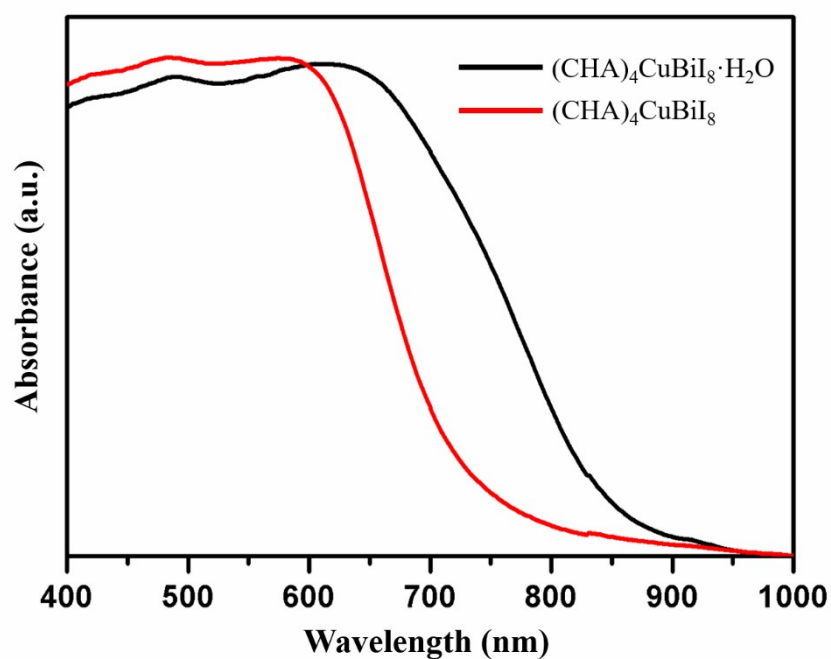
Figure S5. The UV-vis absorption spectra of $(CHA)_4CuBiI_8 \cdot H_2O$ and $(CHA)_4CuBiI_8$ at room temperature.

Table S1. Phase transition temperature and cause of phase transition of $(CHA)_2CdCl_4$, $(CHA)_2PbBr_{4-4x}I_{4x}$ and $(CHA)_2BiCl_5$.

	Phase transition temperature	Cause of phase transition	Ref
$(CHA)_2CdCl_4$	215 K, 367 K	disorder−order transition of cations	1
$(CHA)_2PbBr_{4-4x}I_{4x}$	X=0, T_c=363 K X=0.1125, T_c=378 K X=0.175, T_c=380 K	disorder−order transition of cations	2
$(CHA)_2BiCl_5$	325 K	disorder−order transition of cations	3

Table S2. Crystal data and structure refinements for $(CHA)_4CuBiI_8 \cdot H_2O$ at 150 K, and $(CHA)_4CuBiI_8$ at 400 K and 150 K.

|	$(CHA)_4CuBiI_8 \cdot H_2O$ at 150 K	$(CHA)_4CuBiI_8$ at 400 K	$(CHA)_4CuBiI_8$ at 150 K
Empirical formula	$C_{24}H_{58}BiCuI_8N_4O$	$C_{24}H_{56}BiCuI_8N_4$	$C_{48}H_{112}Bi_2Cu_2I_{16}N_8$
Formula weight	1706.47	1688.46	3376.92
Crystal system	Monoclinic	Monoclinic	Monoclinic
Space group	$C2/c$	$P2_1/c$	Cc
a (Å)	32.3199(9)	9.313(3)	18.7108(11)
b (Å)	8.5589(3)	9.211(4)	17.4002(11)
c (Å)	19.6321(5)	26.573(10)	26.3343(16)
α (°)	90	90	90
β (°)	125.1470(10)	91.149(6)	90.686(3)
γ (°)	90	90	90
Volume(Å^3)	4440.5(2)	2279.0(15)	8573.1(9)
Z	4	2	4
Radiation type	MoK_α	MoK_α	MoK_α
Absorption correction	Multi-scan	Multi-scan	Multi-scan
d_{calc} /g cm^{-3}	2.553	2.460	2.616
F (000)	3096	1528	6112
GOF	1.053	1.047	1.057
$R_1[I > 2\sigma(I)]$	0.0225	0.1152	0.0724
$wR_2[I > 2\sigma(I)]$	0.0585	0.3673	0.1616

Table S3. Selected bond lengths [Å] and bond angles [°] for (CHA)$_4$CuBiI$_8$·H$_2$O at 150 K.

Temperature	bond lengths [Å]		bond angles [°]	
150 K	Bi1—I1	3.0587(2)	I1—Bi1—I1^i	180.0
	Bi1—I1^i	3.0588(2)	I1—Bi1—I3^i	88.137(6)
	Bi1—I3^i	3.0721(2)	I1^i—Bi1—I3^i	91.862(6)
	Bi1—I3	3.0721(2)	I1—Bi1—I3	91.862(6)
	Bi1—I2^i	3.1059(2)	I1^i—Bi1—I3	88.138(6)
	Bi1—I2	3.1059(2)	I3^i—Bi1—I3	180.0
	I3—Cu1	2.7401(13)	I1—Bi1—I2^i	89.908(6)
	I4—Cu1^{ii}	2.4716 (12)	I1^i—Bi1—I2^i	90.092(6)
	I4—Cu1	2.5824 (12)	I3^i—Bi1—I2^i	87.367(6)
			I3—Bi1—I2^i	92.633(6)
			I1—Bi1—I2	90.093(6)
			I1^i—Bi1—I2	89.907(6)
			I3^i—Bi1—I2	92.632(6)
			I3—Bi1—I2	87.368(6)
			I2^i—Bi1—I2	180.0
			Cu1—I3—Bi1	159.20(3)
			Cu1^{ii}—I4—Cu1	32.10(7)
			Cu1^{ii}—Cu1—I4^{ii}	78.31(9)
			Cu1^{ii}—Cu1—I4	69.59(9)
			I4^{ii}—Cu1—I4	142.97(6)
			Cu1^{ii}—Cu1—I3	130.87(4)
			I4^{ii}—Cu1—I3	104.28(4)
			I4—Cu1—I3	110.49(4)

Symmetry codes: (i) −x+1, −y+1, −z+1; (ii) −x+1, y, −z+1/2.

Table S4. Selected bond lengths [Å] and bond angles [°] for (CHA)$_4$CuBiI$_8$ at 400 K.

Temperature	bond lengths [Å]		bond angles [°]	
400 K	Bi1—I2	3.084(2)	I2—Bi1—I2^i	180.0
	Bi1—I2^i	3.084(2)	I2—Bi1—I3	89.93(7)
	Bi1—I3	3.090(2)	I2^i—Bi1—I3	90.07(7)
	Bi1—I3^i	3.090(2)	I2—Bi1—I3^i	90.07(7)
	Bi1—I1^i	3.089(2)	I2^i—Bi1—I3^i	89.93(7)
	Bi1—I1	3.090(2)	I3—Bi1—I3^i	180.0
	Cu1—I4^{ii}	2.403(3)	I2—Bi1—I1^i	87.49(7)
	Cu1—I4	2.403(3)	I2^i—Bi1—I1^i	92.51(7)
	Cu1—I3	3.570(2)	I3—Bi1—I1^i	90.28(6)
			I3^i—Bi1—I1^i	89.72(6)
			I2—Bi1—I1	92.51(7)

I2^i—Bi1—I1	87.49(7)	
I3—Bi1—I1	89.72(6)	
I3^i—Bi1—I1	90.28(6)	
I1^i—Bi1—I1	180.0	
I4^{ii}—Cu1—I4	180.0	
I4^{ii}—Cu1—I3	88.63(7)	
I4—Cu1—I3	91.37(7)	
Bi1—I3—Cu1	159.04(9)	

Symmetry codes: (i) −x+2, −y+1, −z+1; (ii) −x+1, −y, −z+1.

Table S5. Selected bond lengths [Å] and bond angles [°] for (CHA)$_4$CuBiI$_8$ at 150 K.

Temperature	bond lengths [Å]		bond angles [°]	
150 K	Bi1—I7	2.9961(14)	I7—Bi1—I6	89.97(4)
	Bi1—I6	2.9979(14)	I7—Bi1—I5	90.45(4)
	Bi1—I5	3.0797(15)	I6—Bi1—I5	88.64(4)
	Bi1—I4	3.1035(16)	I7—Bi1—I4	90.83(4)
	Bi1—I3	3.1465(14)	I6—Bi1—I4	92.98(4)
	Bi1—I8	3.1601(14)	I5—Bi1—I4	177.93(5)
	Bi2—I14	3.0072(15)	I7—Bi1—I3	179.48(6)
	Bi2—I16	3.0414(14)	I6—Bi1—I3	90.13(4)
	Bi2—I13	3.0877(14)	I5—Bi1—I3	89.04(4)
	Bi2—I11	3.0907(14)	I4—Bi1—I3	89.67(4)
	Bi2—I12	3.1018(17)	I7—Bi1—I8	91.03(4)
	Bi2—I15	3.1410(15)	I6—Bi1—I8	177.99(5)
	Cu1—I1	2.438(8)	I5—Bi1—I8	93.09(4)
	Cu1—I2	2.605(8)	I4—Bi1—I8	85.26(4)
	Cu1—I14^i	2.995(9)	I3—Bi1—I8	88.89(4)
	Cu2—I10	2.458(6)	I14—Bi2—I16	91.40(4)
	Cu2—I9	2.561(7)	I14—Bi2—I13	87.16(4)
	Cu2—I16^i	2.971(9)	I16—Bi2—I13	90.88(4)
	Cu2—I6^{ii}	2.998(8)	I14—Bi2—I11	91.10(4)
	Cu1'—I1	2.5829(12)	I16—Bi2—I11	177.25(5)
	Cu1'—I2	2.5837(12)	I13—Bi2—I11	90.36(4)
	Cu1'—I15^{iii}	2.806(5)	I14—Bi2—I12	93.54(4)
	Cu1'—I3	2.840(5)	I16—Bi2—I12	89.36(4)
	Cu2'—I10	2.555(5)	I13—Bi2—I12	179.26(5)
	Cu2'—I9	2.5905(12)	I11—Bi2—I12	89.37(4)
	Cu2'—I8	2.801(6)	I14—Bi2—I15	178.20(5)
	Cu2'—I11	2.972(8)	I16—Bi2—I15	90.33(4)
	I6—Cu2^{iv}	2.998(8)	I13—Bi2—I15	92.32(4)
	I14—Cu1^v	2.994(9)	I11—Bi2—I15	87.17(4)
	I15—Cu1'^{vi}	2.806(5)	I12—Bi2—I15	86.98(4)
	I16—Cu2^v	2.971(9)	Cu1'—Cu1—I1	78.3(3)

Cu1'—Cu1—I2	72.6(3)
I1—Cu1—I2	150.53(16)
Cu1'—Cu1—I14^i	129.3(6)
I1—Cu1—I14^i	101.6(3)
I2—Cu1—I14^i	100.5(3)
Cu2'—Cu2—I10	76.5(3)
Cu2'—Cu2—I9	74.4(2)
I10—Cu2—I9	149.8(3)
Cu2'—Cu2—I16^i	130.5(5)
I10—Cu2—I16^i	105.3(3)
I9—Cu2—I16^i	99.9(2)
Cu2'—Cu2—I6^{ii}	131.8(5)
I10—Cu2—I6^{ii}	96.4(3)
I9—Cu2—I6^{ii}	96.8(2)
I16^i—Cu2—I6^{ii}	97.5(2)
Cu1—Cu1'—I1	67.6(3)
Cu1—Cu1'—I2	74.2(3)
I1—Cu1'—I2	141.53(13)
Cu1—Cu1'—I15^{iii}	130.2(5)
I1—Cu1'—I15^{iii}	101.87(14)
I2—Cu1'—I15^{iii}	98.76(13)
Cu1—Cu1'—I3	124.0(5)
I1—Cu1'—I3	100.94(12)
I2—Cu1'—I3	104.24(13)
I15^{iii}—Cu1'—I3	105.69(11)
Cu2—Cu2'—I10	69.3(3)
Cu2—Cu2'—I9	72.2(3)
I10—Cu2'—I9	140.6(3)
Cu2—Cu2'—I8	123.9(5)
I10—Cu2'—I8	104.56(16)
I9—Cu2'—I8	103.42(18)
Cu2—Cu2'—I11	131.2(5)
I10—Cu2'—I11	97.83(17)
I9—Cu2'—I11	101.2(2)
I8—Cu2'—I11	104.8(2)
Cu1—I1—Cu1'	34.10(5)
Cu1'—I2—Cu1	33.11(6)
Cu1'—I3—Bi1	167.38(10)
Bi1—I6—Cu2^{iv}	155.74(15)
Cu2'—I8—Bi1	147.36(15)
Cu2—I9—Cu2'	33.35(5)
Cu2—I10—Cu2'	34.23(6)
Cu2'—I11—Bi2	163.34(13)
Cu1^v—I14—Bi2	151.02(16)

Cu1$^{\prime vi}$—I15—Bi2	149.52(9)
Cu2^v—I16—Bi2	161.35(16)

Symmetry codes: (i) x+1/2, y+1/2, z; (ii) x+1/2, y−1/2, z; (iii) x, y+1, z; (iv) x−1/2, y+1/2, z; (v) x−1/2, y−1/2, z; (vi) x, y−1, z.

Table S6. H_{inside}-$I_{outside}$ surface area, mean d_i and mean d_e for $(CHA)_4CuBiI_8 \cdot H_2O$ and $(CHA)_4CuBiI_8$ at different temperatures.

	H_{inside}-$I_{outside}$ surface area (%)	mean d_i	mean d_e
$(CHA)_4CuBiI_8 \cdot H_2O$ 150 K	74.8	2.2272	1.5887
$(CHA)_4CuBiI_8$ 400 K	88.9	2.3618	1.5789
$(CHA)_4CuBiI_8$ 150 K	87.6	2.276	1.5103

References:

1. W.-Q. Liao, H.-Y. Ye, D.-W. Fu, P.-F. Li, L.-Z. Chen and Y. Zhang, *Inorg. Chem.*, 2014, **53**, 11146-11151.

2. H.-Y. Ye, W.-Q. Liao, C.-L. Hu, Y. Zhang, Y.-M. You, J.-G. Mao, P.-F. Li and R.-G. Xiong, *Adv. Mater.*, 2016, **28**, 2579-2586.

3. Y. Wang, S. Han, X. Liu, Z. Wu, Z. Sun, D. Dey, Y. Li and J. Luo, *RSC Adv.*, 2020, **10**, 17492-17496.